



ELSEVIER

Available online at [www.sciencedirect.com](http://www.sciencedirect.com)

SCIENCE @ DIRECT®

C. R. Mecanique 331 (2003) 61–67



## Drop impingement on a deep liquid surface: study of a crater's sinking dynamics

### Impact d'une goutte sur une surface liquide profonde : étude de la dynamique d'enfoncement du cratère

David Brutin

*Polytech' Marseille, Laboratoire IUSTI, Technopôle de Château Gombert, 5, rue Enrico Fermi, 13453 Marseille, France*

Received 6 May 2002; accepted after revision 3 December 2002

Presented by Évariste Sanchez-Palencia

---

#### Abstract

When there is a drop impact on a liquid surface, two phenomena can appear depending on the impact Weber number: either vortex generation or jet formation; in this paper the second behavior is dealt with. Based on the comparison of experimental and theoretical results, the dynamic of splashing drops on deep liquid surfaces is analyzed; this work focuses on the crater's evolution and its maximum. The liquids used are water and ethyl-alcohol. Drop impacts are made with various impact velocities by creating drops from several heights above the liquid surface. A straightforward model to describe and predict the crater's sinking evolution is proposed and agrees well with the experimental results over a range of Weber numbers from 50 to 1500.

**To cite this article:** *D. Brutin, C. R. Mecanique 331 (2003).*

© 2003 Académie des sciences/Éditions scientifiques et médicales Elsevier SAS. All rights reserved.

#### Résumé

Suite à l'un impact d'une goutte sur une surface liquide, deux phénomènes peuvent se produire en fonction du nombre de Weber à l'impact : soit la génération de vortex ou la formation d'un jet. En se basant sur des résultats expérimentaux et un modèle théorique de la dynamique de l'impact d'une goutte sur une surface liquide profonde, l'étude se focalise plus précisément sur l'évolution du cratère et son maximum. Les liquides utilisés sont de l'eau et de l'éthanol. Un modèle pour décrire et prédire l'évolution de l'enfoncement du cratère est proposé et est en bon accord avec les résultats expérimentaux pour une plage de nombre de Weber de 50 à 1500. **Pour citer cet article :** *D. Brutin, C. R. Mecanique 331 (2003).*

© 2003 Académie des sciences/Éditions scientifiques et médicales Elsevier SAS. Tous droits réservés.

**Keywords:** Fluid mechanics; Drop impact; Deep liquid surface; Crater; Modeling

**Mots-clés :** Mécanique des fluides ; Impact de goutte ; Surface liquide profonde ; Cratère ; Modélisation

---

*E-mail address:* [David.Brutin@polytech.univ-mrs.fr](mailto:David.Brutin@polytech.univ-mrs.fr) (D. Brutin).

## Version française abrégée

Quelques études traitent des impacts de gouttes sur des surfaces liquides profondes, le plus souvent les auteurs y détaillent avec des photos l'évolution de la surface libre observée. Ces descriptions de formation de cratères ou de génération de vortex (selon les conditions expérimentales) sont des phénomènes qui interviennent après l'objet de notre étude. La dynamique d'enfoncement du cratère qui a pour origine l'impact d'une goutte sur une surface liquide profonde fait l'objet ici d'un modèle théorique (Section 3.1) validé par des résultats expérimentaux (Section 2.2). Ce modèle se base sur un bilan de quantité de mouvement appliqué à la surface libre déformée. L'équation différentielle du système (Éq. (2)) est résolue de manière à obtenir la solution au maximum de profondeur du cratère (dérivée première de la position nulle). Cette solution sous forme adimensionnée (Éqs. (10)) fait appel au nombre de Weber (Éq. (1a)) et au nombre de Bond (Éq. (10c)). Le modèle qui est en excellent accord avec les résultats expérimentaux pour les deux fluides utilisés ne fait pas intervenir la viscosité du fluide.

## 1. Introduction

In 1908, Worthington [1] observed with a high-speed photography technique an odd but frequent phenomenon: milk drop impacts on shallow milk surfaces. His observations show complex dynamics of the crater's formation due to the drop impingement and droplet emissions all around a thin corona. Different types of drop impacts are described in the literature depending on the type of liquid surface: shallow (less than 10 drop diameters) or deep (more than 50 drop diameters) and other parameters such as the impact drop velocity. Studies deal with the transition behavior such as those of Hsiao et al. [2]. They evidence a critical Weber number for which either vortex generation ( $We_c < 8$ ) or jet formation ( $We_c > 8$ ) will occur. They use mercury and compare their results and criteria to other published values [3–6]. Their explanation is based on the comparison of two characteristic times: that of the surface energy (characteristic time for the drop to deform the surface because of the surface tension) and the convective one (characteristic time for the drop to translate the distance of its diameter); the ratio of these times is the Weber number. Macklin et al. [7] performed experiments of drop impingement on either a deep or a shallow surface and proposed a model to describe the maximum radius of the crater evolution. Their model presents a 'clear' gap between the prediction and their experimental results. Cai [8] reveal a new phenomenon called 'cleavage' when the impact velocities are close to zero. The drop which impacts on the deep liquid surface can either penetrate and fall below the surface or be absorbed just below the surface. These two behaviors appear randomly. Hobbs et al. [9] performed measurements on the spray droplets' number produced by the impact of a water drop on a deep water pool. They focused on the charge-to-mass ratio of these spray droplets and observed the majority of the droplet carry a negative charge. They evidenced that the ratio varies within a defined range. Numerical studies have been also performed to model drop impingement. In 1967, Harlow et al. [10] numerically solved the full Navier–Stokes equations in cylindrical coordinates for drop impingement on deep and shallow pools. Recently, Yarin et al. [11] and Gueyffier et al. [12] focused on drop impingement on shallow surfaces. Yarin et al. observed capillary waves on the liquid film during the drop impingement for specific conditions and Gueyffier et al. observed the typical finger formation during the droplet impact. We focus here on the crater formation dynamics, and more especially on the maximum depth reached by the free surface after the drop impact. We present in this article the experimental results of drop impacts on deep liquid surfaces and propose a model of the crater evolution which is in good agreement with the experimental observations.

## 2. Experiments

### 2.1. Experimental set-up

The experiments reported are carried out in a square transparent PVC<sup>®</sup> tank (0.15 m by 0.15 m wide and 0.18 m high). The tank is completely filled with fluid to allow perfect visualisation of the entire phenomenon through the

transparent faces (below and above the liquid surface). The injector connected to a 0.5 liter syringe using feeder pipes is placed below the surface at a fixed height  $H$  to generate drop impacts at the center of the square observation area. The syringe's piston is connected to a screw and by low angle rotation allows small piston displacements. The injection device is completely filled with fluid. Deionized water ( $\rho_{\text{water}} = 998.7 \text{ Kg} \cdot \text{m}^{-3}$ ,  $\sigma_{\text{water}} = 0.073 \text{ N} \cdot \text{m}^{-1}$ ) and ethyl-alcohol (ethanol) at 99.9% ( $\rho_{\text{ethanol}} = 787.9 \text{ Kg} \cdot \text{m}^{-3}$ ,  $\sigma_{\text{ethanol}} = 0.0226 \text{ N} \cdot \text{m}^{-1}$ ) are used. A high-speed camera is used for the experiments presented. Each film is taken at 360 frames per second with a span of 200 ms. A light is placed behind a 'diffusor plate' in the camera axis.

Before each experiment, the distance between the end of the injector and the liquid surface is noted. The high-speed camera is placed in standby mode. Then, when the liquid surface is checked for stability through the camera a drop is created and kept at the end of the injector for about 5 seconds to ensure no internal convection. The drop is detached from the injector (diameter:  $D_0$ ) by a small, quick movement of the syringe piston by a rotation of the screw. At that moment, the camera is launched into the acquisition mode. After the drop impact the camera is stopped and the film is quickly analyzed to check the good space and time location of the drop impact in the observation area. The procedure is repeated for several heights following a logarithmic law to investigate Weber numbers from 50 to 1500.

## 2.2. Procedure and results

Each film is analyzed by extracting the following information: (a) the experimental impact velocity  $U_0$  by using the frames before the initial drop impact; (b) the crater base diameter; (c) the maximum crater depth of penetration in the liquid  $z_{\text{max}}$ ; (d) the number of droplets expelled. The crater penetration depth is obtained experimentally by measuring in a frame the distance between the free surface before impact at  $t = 0$  ( $z = 0$ ) and the free surface position at a time  $t$ . The maximum is thus experimentally obtained by plotting the free surface location  $z$  as a function of time  $t$ . The experimental and theoretical impact velocities are calculated and checked to be in accordance. In further sections the experimental impact velocity will be used for calculations. Experiments are performed up to the technical set-up's possibilities. For great distances between the end of the injector and the liquid surface ( $H = 1.6 \text{ m}$  for water and  $H = 1 \text{ m}$  for ethyl-alcohol) a disturbing phenomenon called: 'the noise of rain' appears [13].

We take as the beginning of the phenomenon the time when the drop touches the surface. After the drop impact, a hemispheric crater is assumed to be created and it increases to reach a maximum  $z_{\text{max}}$  (experimental observations confirmed this assumption). Then, the free surface rises to form a jet; depending on the operating conditions, droplets can be expelled. Then, the jet sinks to form a second crater which can rise a maximum and can give a second jet if its energy is sufficient. The jet formation results in the crater rising. The crater position  $z$  is obtained by a frame analysis (free surface evolution example in Fig. 1). In the first milliseconds of the phenomenon, the crater is forming. It reaches its maximum after about 20 ms and then rises to generate a jet which also reaches a maximum (about 100 ms after the drop impact). As the jet redescends a droplet is expelled at  $t = 117 \text{ ms}$ . The droplet impacts on the free moving surface at  $t = 170 \text{ ms}$  which generates a second jet formation. The phenomenon finishes about 210 ms after the initial drop impact. We focus here on the first milliseconds just after the impact when the crater is forming, that is, until  $t = 20 \text{ ms}$ . Experimental results of the penetration depth for water and ethyl-alcohol and for all distances of fall are provided in Table 1.

## 3. Theoretical part

A dimensionless number and a characteristic number are defined which will be used in the next section. The inertia and surface tension effects are described by means of the Weber number defined in Eq. (1a) where  $g$  is the

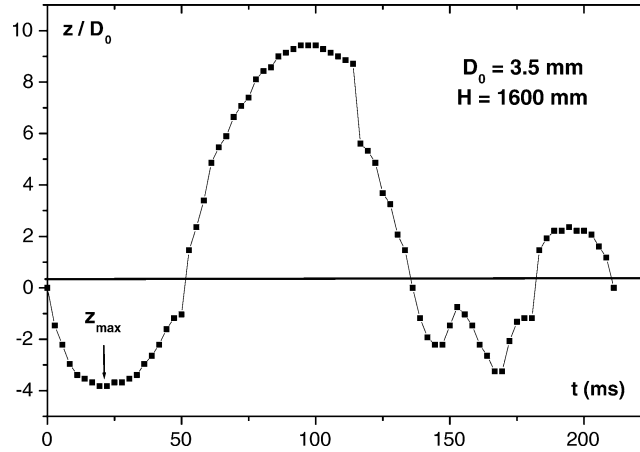
Fig. 1. Free surface evolution for a drop impact at  $t = 0$  ms.Fig. 1. Évolution d'une surface libre pour un impact de goutte à  $t = 0$  ms.

Table 1

Results for all distances of fall  $H$  ( $D_0 = 3.5$  mm for water and 2.3 mm for ethanol)

Tableau 1

Résultats pour les différentes hauteurs  $H$  ( $D_0 = 3,5$  mm pour l'eau et 2,3 mm pour l'éthanol)

Fluid $H$ (mm)	Water		Ethanol	
	$We$	$z/D_0$	$We$	$z/D_0$
33	–	–	49.9	1.97
46	41.2	1.99	70.4	2.27
77	70.3	2.29	118.1	2.57
129	119.2	2.39	198.9	2.57
215	199.0	2.49	337.2	3.03
230	212.1	2.58	356.8	3.03
358	331.3	2.78	558.2	3.17
597	554.9	3.08	934.2	3.48
700	650.6	3.08	1109.3	3.63
996	925.7	3.38	1551.9	3.78
1600	1488.1	3.87	–	–

gravity,  $\rho$  is the density and  $\sigma$  is the surface tension of the liquid investigated. The capillary length  $a$  is also defined with Eq. (1b).

$$(a) We = \frac{\rho U_0^2 D_0}{\sigma}, \quad (b) a = \sqrt{\frac{2\sigma}{\rho g}} \quad (1)$$

### 3.1. Modeling

A model has been elaborated to predict the crater's evolution just after the drop impact. More especially for the milliseconds of the phenomenon when the crater is forming until it reaches its maximum. The model is based on the momentum balance (Eq. (2)) applied to the surface concerned by the fluid displacement. The forces involved in the crater's dynamics are surface tension and gravity. As previously described, the crater is assumed to be

hemispheric. Its radius is thus equal to its depth which will be designated by  $R$  for the dimensioned form and  $r$  for the non-dimensioned form ( $r = R/D_0$ ).

$$\frac{d}{dt}[M(R)U(R)] + 4\pi R\sigma + \rho g R \frac{\pi D_0^2}{4} = 0 \tag{2}$$

The characteristic mass of our system is defined with Eq. (3). The crater can be modeled by the expansion of a half-sphere whose center is the impact point on the surface. So we define the ‘displaced’ mass  $M$  for a crater of radius  $R$  by Eq. (3) where  $M_0$  is the mass of the impacting drop.

$$M(R) = M_0 + \frac{2}{3}\pi\rho R^3 \tag{3}$$

Eq. (2) is put in a dimensionless form to allow an easier analysis using a transformation (Eq. (4)) which gives Eq. (5a) where  $G$  is defined in Eq. (5b).  $r$  is the non-dimensioned position and  $\dot{r} = dr/dt$  is the first time derivative of the non-dimensioned position.

$$\frac{d}{dt} = \frac{dr}{dt} \frac{d}{dr}, \tag{4}$$

$$(a) \dot{r} \frac{d\dot{r}}{dr} + 4\dot{r} \frac{d}{dr}(r^3\dot{r}) = -12r \left(\frac{a}{D_0}\right)^3 (1 + G), \quad (b) G = \frac{1}{8} \left(\frac{D_0}{a}\right)^2 \tag{5}$$

Eq. (5) is similar to the Rayleigh–Plesset equation in sonoluminescence and bubble cavitation. For our situation, Eq. (5) consists for the left-hand of two contributions from the momentum balance: the first term is the initial crater momentum which translates the drop impact on the surface and the second term is the momentum of the crater sinking under the deep liquid surface, whereas the right-hand consist of the capillary and gravity contributions. Because Eq. (5) cannot be solved analytically, 2 cases are considered:

- (a) if  $r \ll 1$  in Eq. (5) the second member of the left part is negligible and Eq. (5) gives Eq. (6a);
- (b) if  $r \gg 1$  in Eq. (5) the first member of the left part is negligible and Eq. (5) gives Eq. (6b).

$$(a) (r^3\dot{r})^2 = C - \frac{6}{5} \left(\frac{a}{D_0}\right)^3 (1 + G)r^5, \quad (b) \dot{r}^2 = \tilde{U}_0^2 - 12 \left(\frac{a}{D_0}\right)^3 (1 + G)r^2 \tag{6}$$

$C$  is an integration constant found by coupling Eqs. (6a) and (6b) at initial conditions ( $r = 1$  and  $\dot{r} = \tilde{U}_0$ ) given by Eq. (7a).  $\tilde{U}_0$  is the non-dimensional impact velocity given by Eq. (7b).

$$(a) C = \tilde{U}_0^2 + \frac{6}{5} \left(\frac{a}{D_0}\right)^3 (1 + G), \quad (b) \tilde{U}_0 = U_0 \sqrt{\frac{\rho D_0}{\sigma}} \tag{7}$$

To obtain the penetration depth equation, Eq. (6a) and Eq. (7a) are coupled to give the crater evolution equation (Eq. (8)).

$$(r^3\dot{r})^2 = \tilde{U}_0^2 + \frac{6}{5} \left(\frac{a}{D_0}\right)^3 (1 + G)(1 - r^5) \tag{8}$$

At  $\dot{r} = 0$  and  $r = z_{\max}/D_0$ , it is possible to extract the maximum depth of penetration expression (Eq. (9)).

$$\frac{z_{\max}}{D_0} = \left(1 + \frac{5}{6} \left(\frac{D_0}{a}\right)^3 \frac{\tilde{U}_0^2}{1 + G}\right)^{1/5} \tag{9}$$

The maximum depth of penetration is given by Eqs. (10).

$$(a) \frac{z_{\max}}{D_0} = (1 + kWe)^{1/5}, \quad (b) k = \frac{20Bo^3}{24 + 3Bo^2}, \quad (c) Bo = \frac{D_0}{a} \tag{10}$$

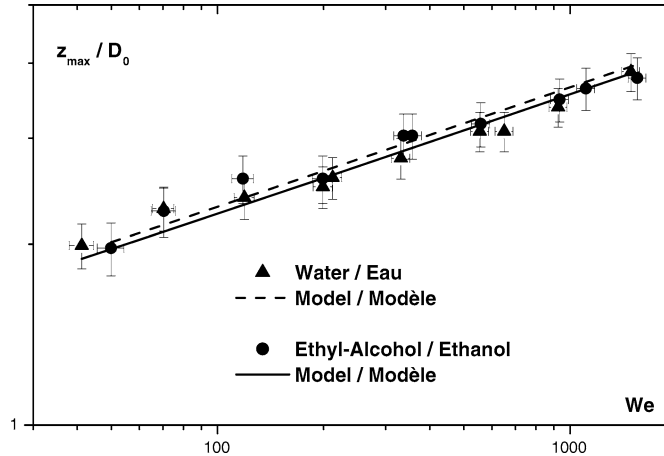


Fig. 2. Experimental points and theoretical prediction.

Fig. 2. Points expérimentaux et prédiction théorique.

### 3.2. Comparaison

In Fig. 2 the relative location of the data in Table 1 is presented. For both fluids, the experimental slopes are virtually identical. To compare with the model,  $k$  is evaluated:  $k_{\text{water}} = 0.563$ ,  $k_{\text{ethyl-alcohol}} = 0.644$ . Both  $k$  are quite identical. This can be explained in Eq. (10b) by the ratio of the drop diameter to the capillary length. For water and ethyl-alcohol and our experiments, it appears that this ratio is quite identical below 1 (0.91 for water and 0.95 for ethyl-alcohol). The driving parameter between two fluids for the maximum depth's prediction is thus this characteristic ratio which is also the Bond number.

By comparison between the experimental and theoretical evolutions, it is possible to note that both results provide identical slopes and are in good agreement. The prediction from the model previously presented in Fig. 2 provides a good estimation of the crater's maximum depth. Note the model prediction does not take into account the fluid viscosity. As a result viscosity is a minor contribution in the momentum equation.

This theoretical modeling has been experimentally validated in a Weber number range of about 50 to 1500. For the lower boundary, no crater develops under a critical Weber number found experimentally by Hsiao et al. [2] ( $We_C \sim 8$ ) whereas for the upper boundary, a 'noise of rain' phenomenon [13] of air bubble injection under the surface perturbs the crater's sinking for Weber numbers higher than 1500.

## 4. Conclusion

A model is proposed to describe the crater's evolution and its maximum after a drop impact on a deep liquid surface. Experimental results are obtained with water and ethyl-alcohol and agree well with the theoretical prediction. An original aspect of the model is that the crater's maximum depth prediction only uses Weber and Bond numbers but does not use the fluid viscosity. The crater's sinking and peak formation only develop in a range of Weber numbers whose boundaries have been determined by other studies [2,13]; within this domain our model predicted well the maximum crater depth variation. A comparison between the experimental and theoretical sinking evolution of the crater just after the drop impact is currently under investigation.

## References

- [1] A.M. Worthington, A Study of Splashes, Longmans, Green, London, 1908.
- [2] L.G. Quintero, M. Hsiao, S. Lichter, The critical weber number for vortex and jet formation for drops impinging on a liquid pool, *Phys. Fluids* 31 (1988) 3560–3562.
- [3] R. Mesler, F. Rodriguez, *J. Colloid Interface Sci.* 106 (347) (1985).
- [4] R. Mesler, F. Rodriguez, *J. Colloid Interface Sci.* 121 (121) (1988).
- [5] P.R. Critchlow, D.S. Chapman, *J. Fluid Mech.* 29 (177) (1967).
- [6] H.F. Newall, J.J. Thomson, *Proc. Roy. Soc. London* 39 (417) (1885).
- [7] G.J. Metexas, W.C. Macklin, Splashing of drops on liquid layers, *J. Appl. Phys.* 47 (1976) 3963–3970.
- [8] Y.K. Cai, Phenomena of a liquid drop falling to a liquid surface, *Experiment. Fluids* 7 (1989) 388–394.
- [9] P.V. Hobbs, A.J. Kezweeny, Splashing water drop, *Science* 155 (1967) 1112–1114.
- [10] F.H. Harlow, J.P. Shannon, The splash of a liquid drop, *J. Appl. Phys.* 38 (1967) 3855–3866.
- [11] D.A. Weiss, A.L. Yarin, Single drop impact onto liquid films: neck distortion, jetting, tiny bubble entrainment, and crown formation, *J. Fluid Mech.* 385 (1999) 229–254.
- [12] D. Gueyffier, S. Zaleski, Formation de digitations lors de l’impact d’une goutte sur un film liquide, *C. R. Acad. Sci. Paris Sér. IIB* 326 (1998) 839–844.
- [13] H.N. Oguz, A. Prosperetti, The impact of drops on liquid surfaces and the underwater noise of rain, *Annual Rev. Fluid Mech.* 25 (1993) 557–602.